Live fast and die young

Evolution and fate of massive stars

Renzo, M.

Publication date
2019

Document Version
Other version

License
Other

Pulsational pair-instability supernovae in very close binaries

C

C.1 Time dependent convection

During phases of dynamical instability large regions in the star can switch back and forth between being stable or unstable to convection on timescales comparable to or shorter than a convective turnover timescale. To properly treat energy transport under these conditions, a model for time-dependent convection is required. Here we describe a simple model that captures the relevant timescales and reduces to standard mixing-length theory (MLT, Böhm-Vitense 1958) in long timescales. We follow the work of Arnett (1969) and consider the average convective velocity v_c in MLT to be an independent variable which satisfies the equation

$$\frac{\partial v_c}{\partial t} = \frac{v_{\rm MLT}^2 - v_c^2}{\lambda}, \quad \text{for convectively unstable regions} \tag{C.1}$$

where $v_{\rm MLT}$ is the steady state value predicted by MLT. λ is the mixing length, which we define as $\alpha_{\rm MLT} H_P$ where $\alpha_{\rm MLT}$ is a free parameter of order unity and H_P is the local pressure scale height. In particular for our simulations we use $\alpha_{\rm MLT} = 2$. On timescales much longer than a convective turnover timescale ($\tau_{\rm to} = \lambda / v_{\rm MLT}$) convective velocities asymptotically approach the steady state value $v_{\rm MLT}$, recovering standard MLT. In regions that are convectively stable $v_{\rm MLT} = 0$ and simply using Equation (C.1) would result in convective velocities decaying on a timescale $\tau = \lambda / v_c$ which becomes infinetely large as convective velocities are reduced. This ignores the actual timescale in which fluid parcels would be slowed down in a stratified medium. To provide an order of magnitude correction to this, we construct a timescale $\tau_N = 1/N$ where N is the Brunt-Väisällä frequency and use

$$\frac{\partial v_c}{\partial t} = -\frac{v_c^2}{\lambda} - \frac{v_c}{\tau_N}, \quad \text{for convectively stable regions} \tag{C.2}$$

to model the shutoff of convection. Mixing from convection is modeled as a diffusive process with a diffusion coefficient $D = v_c \lambda / 3$.

In its standard form, MLT solves an algebraic system of three equations to compute the steady state convective velocity $v_{\rm MLT}$, the temperature gradient of the star ∇, and the temperature gradient of displaced blobs of material ∇', which differs from the adiabatic gradient ∇_a due to radiative energy losses. In our case, we require a derivation of MLT for a given value

of v_c rather than the steady state one. Following Cox & Giuli (1968), if convective velocities are given then the convective efficiency Γ (which is the ratio of energy radiated by a moving parcel, to the energy released when it dissolves after crossing a mixing length) can be directly computed as

$$\Gamma = \frac{c_P}{6ac}\frac{\kappa\rho^2 v_c \lambda}{T^3}. \tag{C.3}$$

Using this, the values of ∇ and ∇' can be determined from

$$\nabla_r = \nabla - \frac{9}{4}\Gamma(\nabla - \nabla'), \qquad \frac{\nabla_r - \nabla}{\nabla_r - \nabla_a} = \frac{9\Gamma^2/4}{1 + \Gamma(1 + 9\Gamma/4)}, \tag{C.4}$$

where ∇_r is the radiative temperature gradient. All of these are standard results of MLT (cf. Cox & Giuli 1968), but we have taken care here to only use expressions that do not assume a steady state value for v_c in order to have a self-consistent model. Although this model incorporates the timescales relevant to the process, it does not intend to solve some of the long-standing problems with MLT (see Arnett et al. 2018a for a recent discussion). For instance, our model does not incorporate overshooting directly but instead uses an exponentially decaying mixing coefficient beyond convective regions (see Section 5.2) which does not account for energy transport. Also, sharp composition gradients near convective boundaries can lead to discontinuities in the Brunt-Väisälä frequency, producing a discontinuous $\partial v_c/\partial t$ and v_c at a convective boundary. Under these circumstances we would expect turbulent energy to be transported through the boundary, but our model does not include this effect.

C.2 Resolution and nuclear reaction network convergence test

In order to test if our results are converged, we have performed a test using the first pulse of our $84M_\odot$ model. Using our default setup, at the onset of the pulse this star has $58.1M_\odot$ and after the first mass ejection ends up with a mass of $41.49M_\odot$. During this phase, the model is resolved using between $\sim 2500 - 3500$ cells and ~ 6000 timesteps. To test the convergence of our model to changes in spatial and temporal resolution, we have computed a model that after helium depletion approximately doubles both.

During the pulsational phase we use the approx21 reaction network for which the isotopes and linkages are shown in Figure C.1. The backbone is a strict α-chain composed of (α,γ) and (γ,α) links among the 13 isotopes ^{4}He, ^{12}C, ^{16}O, ^{20}Ne, ^{24}Mg, ^{28}Si, ^{32}S, ^{36}Ar, ^{40}Ca, ^{44}Ti, ^{48}Cr, ^{52}Fe, and ^{56}Ni. Above $\simeq 2.5\times10^9$ K is it essential to include (α,p)(p,γ) and (γ,p)(p,α) links in order to obtain reasonably accurate energy generation rates and abundances (Timmes & Swesty 2000). At these elevated temperatures the flows through the (α,p)(p,γ) sequences are faster than the flows through the (α,γ) channels. An (α,p)(p,γ) sequence is, effectively, an (α,γ) reaction through an intermediate isotope. Approx21 includes 8 (α,p)(p,γ)

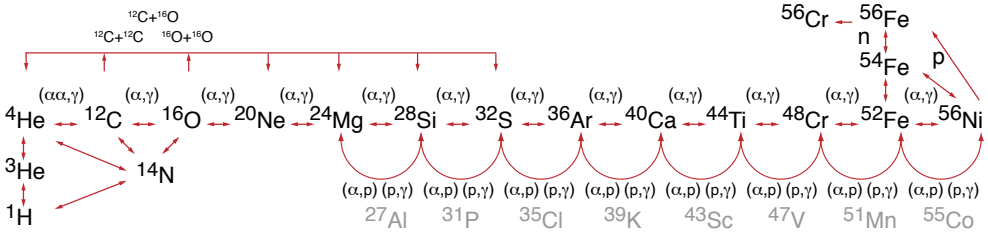

Fig. C.1: List of isotopes and linkages in the approx21 network used during late burning stages in our calculations.

sequences and their inverses by assuming steady-state proton flows through the intermediate isotopes ^{27}Al, ^{31}P, ^{35}Cl, ^{39}K, ^{43}Sc, ^{47}V, ^{51}Mn, and ^{55}Co . The assumed steady-state proton flows allows inclusion of the (α,p)(p,γ) sequences without explicitly evolving the proton or intermediate isotope abundances. In addition to this α-chain backbone, approx21 includes approximations for steady-state hydrogen burning (PP chain and CNO cycle), carbon and oxygen burning (^{12}C+^{12}C, ^{12}C+^{16}O, ^{16}O+^{16}O), and aspects of photodisintegration with ^{54}Fe. These additions are briefly described in Weaver et al. (1978). Finally, approx21 adds the ^{56}Cr and ^{56}Fe isotopes and tuned steady-state reaction sequences to attain a reasonably accurate lower electron fraction Y_e (as compared to much larger reaction networks) for presupernova models (Paxton et al. 2015). To test the accuracy of this few-isotope network during a pulse we have also computed the first pulse of our $84M_\odot$ model using the 203 isotope network of Renzo et al. (2017) which is tuned to properly capture silicon burning.

Figure C.2 shows the results of our convergence tests. For ease of comparison between the simulations, we have matched all tracks in time to the point where the first pulsation reaches its maximum central temperature, and we compare values 100000 seconds after this point. Overall the three simulations are quantitatively consistent, with relative differences in the kinetic energy of ejected layers and final masses of around 6%. Final central temperatures digress by around 15%, but considering that during the pulse it is lowered by a factor of ~ 30, this is a small error. Given these results, and that we do not study detailed nucleosynthetic yields of PPISN or PISN in this work, we consider our choice of resolution and nuclear reaction network appropriate. In particular, the use of approx21 instead of the 203 isotope network reduces the runtime of each model by more than a factor of 10, significantly lowering the cost of our simulations.

As a more extreme example, we repeat this exercise for a PISN model with an initial mass of $M_i = 200M_\odot$, which is shown in Figure C.3. This model is near the upper end of the mass range of PISN, with $M_{\text{pre SN}} = 108.4$, and during the explosion reaches a central temperature of 5.2×10^9 K, significantly higher than the first pulse of the PPISN model shown before, which reaches a maximum temperature of 3.2×10^9 K. The model with the approx21 network produces a total of $25.9M_\odot$ of ^{56}Ni, which is $\sim$ 13% lower than that produced by the model with the 203 isotope network. The error on the kinetic energy of the ejecta is similar to that of the PPISN model, with the 203 isotope network predicting an ejecta energy $\sim$ 4% larger

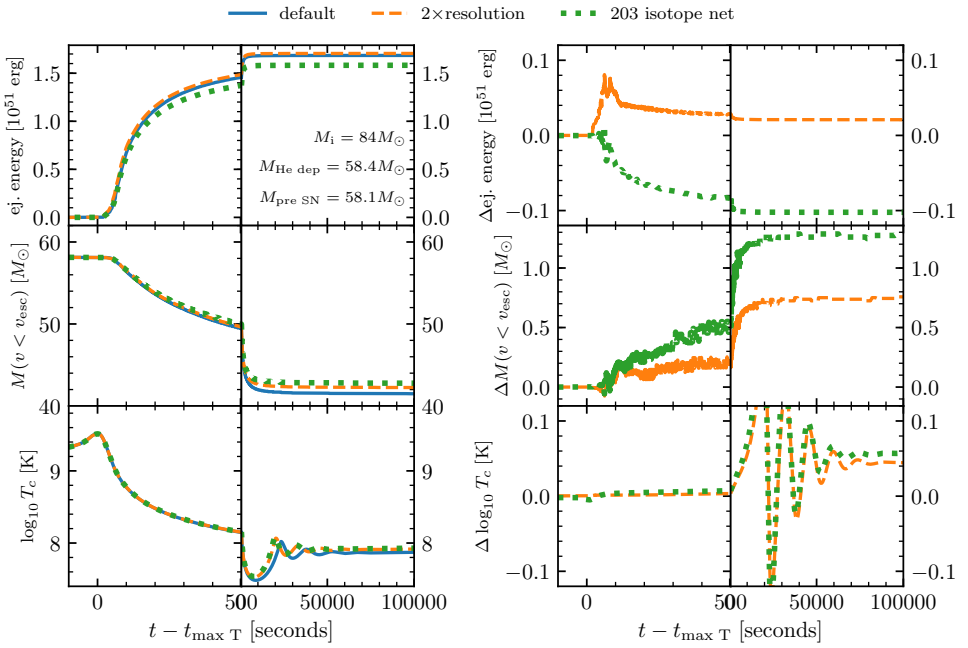

Fig. C.2: (left) Evolution of the kinetic energy of ejected layers, the mass at velocities below the escape velocity and central temperature for the first pulse of an $M_{\rm i} = 84M_{\odot}$ progenitor. Results are shown for the default set of parameters used in this paper, a simulation with double the resolution in time and space, and one with a 203 isotope network rather than the default 21 isotope network we use for all other models. (right) For the simulations with higher resolution and a bigger network, each line shows how the difference with respect to the simulation with our default choice of parameters evolves with time.

than that of the approx21 model. We see that the dynamics of the explosion are consistently reproduced, although the difference in Nickel mass would produce non-negligible differences on the resulting lightcurves. Our focus however is on the evolution of PPISN, which do not produce significant amounts of Nickel, so we still consider the use of approx21 to be justified.

C.3 Precision of the relaxation procedure

To model the long-lived phases between pulses in our more massive progenitors, we use a relaxation procedure that creates a hydrostatic model from scratch that matches the mass, entropy and composition profile after the pulse. This method has been described in Appendix B of Paxton et al. (2018) and here we show how well it reproduces the pre-relaxation model. In order to perform a relaxation after a pulse, we require that velocities are below 20 km s^{-1} and no layers are moving at more than 50% their local sound speed within the inner 99% of mass that remains bound. To prevent the relaxation happening when these thresholds are

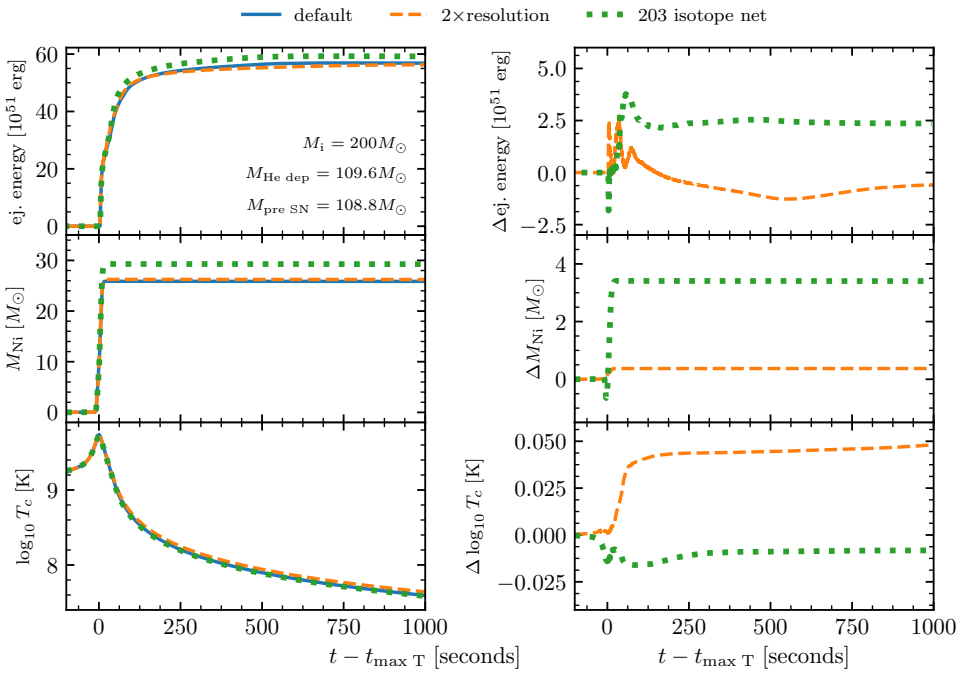

Fig. C.3: Same as Figure C.2, but for a PISN model with $M_i = 200M_\odot$ ($M_{\rm pre\ SN} = 108.4M_\odot$), and showing the evolution of the total mass of ^{56}Ni instead of the ejected mass.

satisfied during minima and maxima of oscillations, we require these to be satisfied for at least 100 continuous timesteps. We also require the neutrino and nuclear burning luminosities to be below $10^{11}L_\odot$ and $10^{10}L_\odot$ respectively, in order to avoid relaxing the model when the core is evolving on a timescale of ∼days.

Figure C.4 shows the outcome of two relaxation procedures done for the $76M_\odot$ model shown in Figure 5.2 after the first and fourth pulses. For all other three pulses shown, the conditions on the luminosities are not satisfied, so the model is evolved further without removing the outer layers. As it can be seen, except for the very outermost layers temperatures are matched very accurately in the relaxed model, with the central temperature differing by 0.0002 and 0.0005 dex for the first and fourth pulse respectively. As expected, the very outermost layers show more noticeable differences, with clear digressions being visible at the outer $\sim 0.2M_\odot$ and $\sim 0.05M_\odot$ after the first and fourth pulse respectively. Although a difference is expected, since the very outermost layers are still falling back when the relaxation is made, we do care about accurately characterizing observable properties of the star in between pulses. However, the discrepancy turns out to be not very important. After the first pulse, the thermal timescale of the outer $0.2M_\odot$ is just of 1.4 years, a very small time compared to the

almost 3 millennia between the first and second pulse. This means that although we do not trust the effective temperature and luminosity of our models immediately after a pulse, after ~ 1 year any anomalies from relaxation in the outermost layers will be removed.

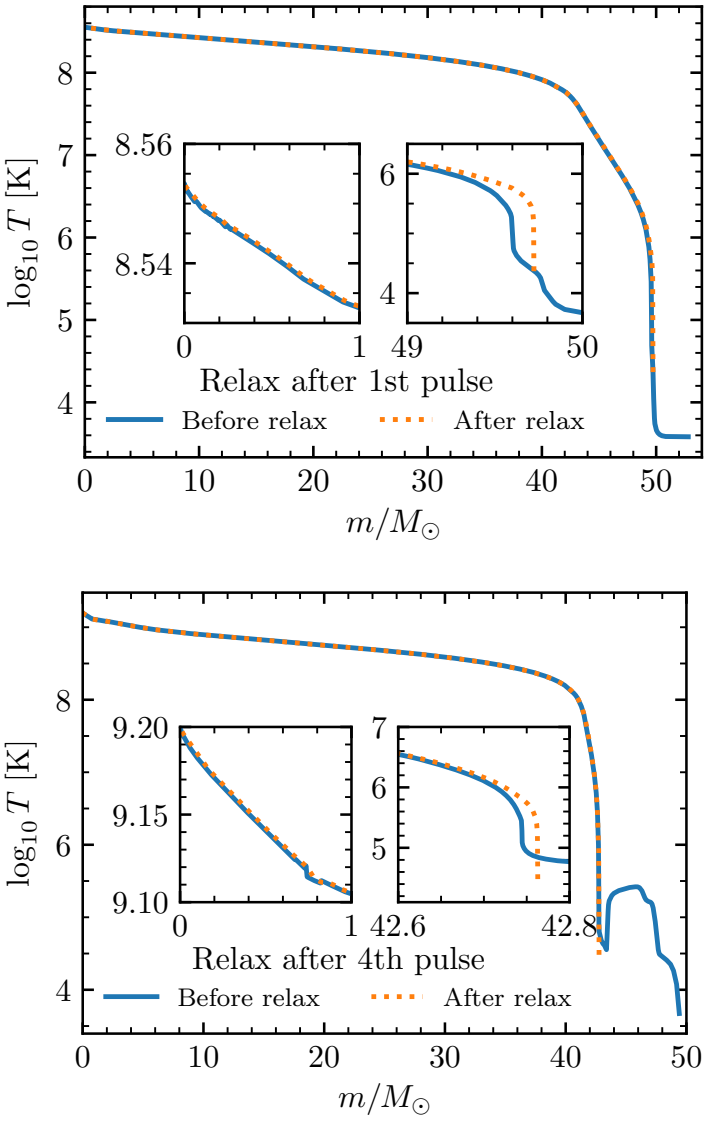

Fig. C.4: Pre and post-relaxation temperature profiles for our $M_i = 76M_\odot$ model after the first and fourth pulses.